

## Electronic Supplementary Information

### Synchronous Dimension- Crystallization Engineering Enables Highly Efficient 2D/3D Tin Perovskite Solar Cells

Ziyong Kang,<sup>a</sup> Peng Feng,<sup>b</sup> Kun Wang,<sup>\*c</sup> Lu Zhang,<sup>d</sup> Rui Meng,<sup>a</sup> Yali Chen,<sup>a</sup> Jiandong Wu,<sup>a</sup> Feng Yang,<sup>a</sup> Xuewen Zhang,<sup>b</sup> Tianxiang Li,<sup>a</sup> Jingzhi Shang,<sup>b</sup> Yu Tong,<sup>\*a</sup> Hongqiang Wang<sup>\*a</sup>

<sup>a</sup> State Key Laboratory of Solidification Processing, Center for Nano Energy Materials, School of Materials Science and Engineering, Northwestern Polytechnical University, Xi'an 710072, China.

<sup>b</sup> Frontier Science Center for Flexible Electronics, Xi'an Institute of Flexible Electronics, Northwestern Polytechnical University, 127 Youyi West Road, Xi'an, Shaanxi, 710072, P.R. China.

<sup>c</sup> School of microelectronics, Northwestern Polytechnical University, Xi'an 710072, China.

<sup>d</sup> Key Laboratory of Applied Surface and Colloid Chemistry Ministry of Education, Shaanxi Key Laboratory for Advanced Energy Devices, Shaanxi, Engineering Lab for Advanced Energy Technology, School of Materials Science Engineering Shaanxi Normal University, Xi'an 710119, P. R. China.

E-mail: kunwang@nwpu.edu.cn; yutong@nwpu.edu.cn; hongqiang.wang@nwpu.edu.cn.

## Experimental Section

### Materials

Formamidinium iodide (FAI, 99.5%) and phenethylammonium Chloride (PEACl, 99.5%) were purchased from Xi'an Yuri Solar Co. Ltd. Tin (II) iodide ( $\text{SnI}_2$ , 99.999%) was purchased from 3A Materials, Tin(II) Fluoride ( $\text{SnF}_2$ , 99.9%), Tin powder (99.5%), 4-Guanidinobenzoic acid hydrochloride (GBAC, 97%), and Ammonium thiocyanate ( $\text{NH}_4\text{SCN}$ , 99.99%) were purchased from Aladdin, 1-(3-methoxycarbonyl)-propyl-1-phenyl-(6, 6) C61 (PCBM) and bathocuproine (BCP) were purchased from 3A Nano-C, respectively. Tin (IV) oxide ( $\text{SnO}_2$ , 99%) was purchased from Alfa Aesar, 2,2',7,7'-Tetrakis [N, N-di(4-methoxyphenyl) amino]-9,9'-spirobifluorene (Spiro-MeOTAD, 99%), Dimethyl sulfoxide (DMSO, 99.9%), N, N-dimethylformamide (DMF, 99.8%), Iso-Propyl Alcohol (IPA, 99.5%), and chlorobenzene (CB, 99.8%) were obtained from Sigma-Aldrich. PEDOT: PSS (Chevios AL4083) was purchased from J&K Chemical. All the above chemicals were used as received without any further purification. Toluene (99.8%) was purchased from Ourchem and contained with a molecular sieve to remove water.

### Precursor solution

The perovskite precursor solution ( $\text{PEA}_{0.15}\text{FA}_{0.85}\text{SnI}_{2.85}\text{Cl}_{0.15}$ ) was prepared by dissolving 65.79 mg FAI (0.3825 mmol), 10.64 mg PEACl (0.0675 mmol), 167.63 mg  $\text{SnI}_2$  (0.45 mmol), 7.05 mg  $\text{SnF}_2$  (0.09 mmol), 1.71 mg  $\text{NH}_4\text{SCN}$  (0.0225 mmol), 2.81 mg Sn powder (0.0225 mmol) and different concentrations of GBAC, into a mixed solvent of 100  $\mu\text{L}$  DMSO and 400  $\mu\text{L}$  DMF and then stirring for about 12 h.

### Device Fabrication

The tin PSCs were fabricated with a configuration of ITO/PEDOT: PSS/perovskite/PCBM/BCP/Ag. ITO glass substrates were ultrasonically cleaned with detergent, deionized water, ethyl alcohol, acetone, and isopropanol for 60 min, respectively. Then, the cleaned ITO glass substrates were cleaned with oxygen plasma (Harrick PDC-32G) for 20 min. PEDOT: PSS was spin-coated on ITO substrates at 5000 rpm for 45 s and annealed at 140 °C for 20 min in air. After cooling, the tin perovskite precursor solution was spun at 1000 rpm for 10 s, followed by 5000 rpm for 30 s in the glove box. Toluene was dripped onto the perovskite film 10 s after the rotation speed was increased to 5000 rpm, following with annealing at 70 °C for 10 min. Then, the electron transport layer was prepared by spin-coating the PCBM solution (30 mg/mL in CB) at 1800 rpm for 30 s and annealed at 70 °C for 10 min. Finally, a 5 nm thick BCP and 110 nm thick Ag was deposited using a vacuum thermal coater (Suzhou Fang Sheng OMV-FS200). The size of the tin PSCs is 0.05  $\text{cm}^2$ , which is determined by the overlapping area of the ITO and Ag contact.

### Devices Characterization

The XRD patterns were determined by an X-ray diffractometer (AXS D8 Advanced, Bruker, Germany) with monochromatic  $\text{Cu K}\alpha$  radiation. The morphology of the perovskite film was measured by a field emission scanning electron microscope (SEM) (ZEISS Sigma 300, Germany). Atomic force microscopy (AFM) was performed using Dimension Icon microscope (Bruker, Germany). Ultraviolet-visible (UV-vis) absorption measurement was obtained by the UV-LAMBDA 365 spectrophotometer. The PL were characterized using an Edinburg Instruments FLS 980. Microscopic PL mappings were taken with a confocal spectroscopic system (South Port, Jade Mat), where a 532 nm continuous-wave laser was used as the excitation source together with a  $\times 50$  objective lens ( $\text{NA} = 0.8$ ). The TRPL spectra were collected using a Delta Flex modular fluorescence lifetime system by Horiba Scientific. The X-ray photoelectron spectroscopy (XPS) was tested by the PHI-5000 Versa Probe III. The ultraviolet photoelectron spectroscopy (UPS) of perovskite films were measured by an Axis Supra (Kratos). The J-V curves were measured using a Xenon-lamp-based solar simulator (Oriel 67005, 150 W Solar Simulator) with a source meter (Keithley 2420 Source-Meter) under illumination at AM 1.5G (100  $\text{mW cm}^{-2}$ ). The light intensity was calibrated with a monocrystalline silicon reference cell (Hamamatsu S1133). All the devices were tested in a nitrogen-filled glovebox. The external quantum efficiency (EQE) was characterized by using an Enlitech EQE measurement system (QE-R3011). The electrical impedance spectroscopy (EIS) was measured by using an electrochemical workstation (Chenhua CHI660E). A Keithley 2420 Source-Meter was used to measure the relevant I-V curves. GIWAXS measurement was performed by employing a beam energy of 10 keV and a PILATUS detector at the BL02U2 and BL03HB beamline of Shanghai Synchrotron Radiation Facility (SSRF), Shanghai, China. Fourier transform infrared (FTIR) spectra were recorded using a Thermo-Nicolet iS5 instrument. In situ fluorescence spectra were recorded in a  $\text{N}_2$  glovebox, and the excited light was at 365 nm from a UV lamp. TA spectra measurements were conducted by utilizing a TA system (Time-Tech Spectra, LLC) equipped with a high-speed spectrometer (Ultrafast systems, HELIOS) and a regeneratively amplified laser (Light conversion, 1030 nm, 230 fs and 100 kHz repetition). The diode-pumped all-solid-state femtosecond Yb: YAG laser is equipped with a wavelength of 1030 nm, a matching repetition frequency of 100 kHz, and a pulse width of 230 fs.

### Theoretical Computation

DFT calculations were performed employing the Vienna Ab Initio Simulation Package (VASP). The interaction between valence electrons and ions were described by the projector-augmented wave (PAW) method<sup>11</sup>. The exchange correlation of the Kohn-Sham equation was presented by generalized gradient approximation (GGA) with the Perdew-Burke-Ernzerhof (PBE) functional, and Grimme's DFT-D3 method to include the effect of weak van der Waals (vdW) interactions. A plane-wave basic set was used to expand the wavefunctions with the kinetic cutoff energy set to 550 eV. A plane-wave basic set was used to expand the wavefunctions with the kinetic cutoff energy set to 550 eV. For the calculations of slabs, a  $2\times 2\times 1$  (DMF and GBAC),  $2\times 1\times 1$  ( $\text{SnI}_2$ ),  $4\times 2\times 1$  (FAI) Monkhorst-Pack k-point grid was implemented to sample the Brillouin zone. During

the geometry optimization, the convergence criteria for the atomic forces and the total energies were set to 0.02 eV/Å and 10<sup>-4</sup> eV, respectively. The adsorption energy ( $E_{ad}$ ) was defined by:

$$E_{ad} = E_{Total} - E_{Surface} - E_{Adsorbate}$$

where  $E_{Total}$ ,  $E_{Surface}$  and  $E_{Adsorbate}$  are the total energies of the optimized surface with adsorbate, the surface, and adsorbate in the gas phase.

For the calculations of slabs, a 2×2×1 (DMF and GBAC), 2×1×1 (SnI<sub>2</sub>), 4×2×1 (FAI) Monkhorst-Pack k-point grid was implemented to sample the Brillouin zone. During the geometry optimization, the convergence criteria for the atomic forces and the total energies were set to 0.02 eV/Å and 10<sup>-4</sup> eV, respectively.

### Computational methods

#### Electrical conductivity Calculation

The conductivity of perovskite film from the current-voltage (I-V) characteristic curves was calculated by eq. 1<sup>2</sup>

$$\sigma = \frac{I}{V} \times \frac{d}{S} \quad (1)$$

where  $\frac{I}{V}$  is the slope of lines in conductivity, d and S are the thickness and area of perovskite film

#### Exciton lifetime calculation

The exciton lifetime of the perovskite films can be derived from the femtosecond transient absorption spectroscopy (TAS) by a bi-exponential fitting as shown in eq.2<sup>3</sup>

$$y = A_1 e^{\left(-\frac{t}{\tau_1}\right)} + A_2 e^{\left(-\frac{t}{\tau_2}\right)} \quad (2)$$

where  $\tau$  is the exciton lifetime,  $\tau_1$  and  $\tau_2$  are the decay components of the trap-assisted and radiative recombination process respectively. The carrier recombination lifetime can be calculated by eq.3

$$\tau = \frac{A_1 \tau_1^2 + A_2 \tau_2^2}{A_1 \tau_1 + A_2 \tau_2} \quad (3)$$

#### Carrier recombination lifetimes calculation

The carrier recombination lifetimes can be derived from the time-resolved photoluminescence (TRPL) by a bi-exponential fitting as shown in eq.4<sup>4</sup>

$$Y = A_1 e^{\left(-\frac{t}{\tau_1}\right)} + A_2 e^{\left(-\frac{t}{\tau_2}\right)} \quad (4)$$

where  $\tau$  is the carrier recombination lifetime,  $\tau_1$  and  $\tau_2$  are the decay components of the trap-assisted and radiative recombination process respectively. The carrier recombination lifetime can be calculated by eq.5

$$\tau = \frac{A_1 \tau_1^2 + A_2 \tau_2^2}{A_1 \tau_1 + A_2 \tau_2} \quad (5)$$

#### Analysis of space-charge-limited current (SCLC) model

The trap density ( $N_t$ ) of perovskite films from the dark J-V curves of the electron-only and hole-only devices can be calculated by eq.6<sup>5</sup>

$$N_t = \frac{2\epsilon\epsilon_0 V_{TFL}}{qd^2} \quad (6)$$

where q is the electron charge, d is the thickness of perovskite film,  $\epsilon_0$  and  $\epsilon$  are the vacuum permittivity and relative dielectric constant of perovskite, and  $V_{TFL}$  is ordinate of the intersection of ohmic region and trap-filling limited region.

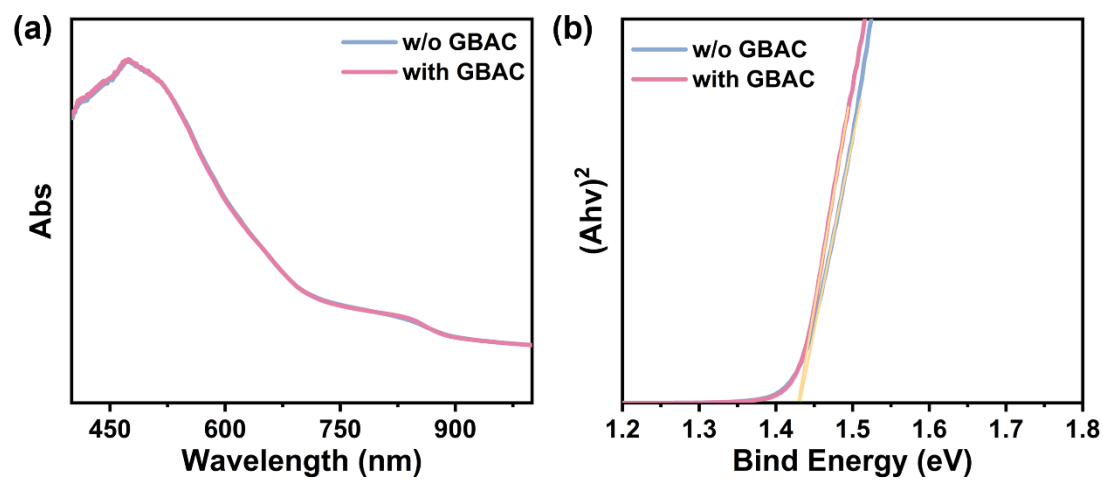


Fig. S1 (a) UV-vis absorption spectra, and (b) Tauc-plot of perovskite films without and with GBAC.

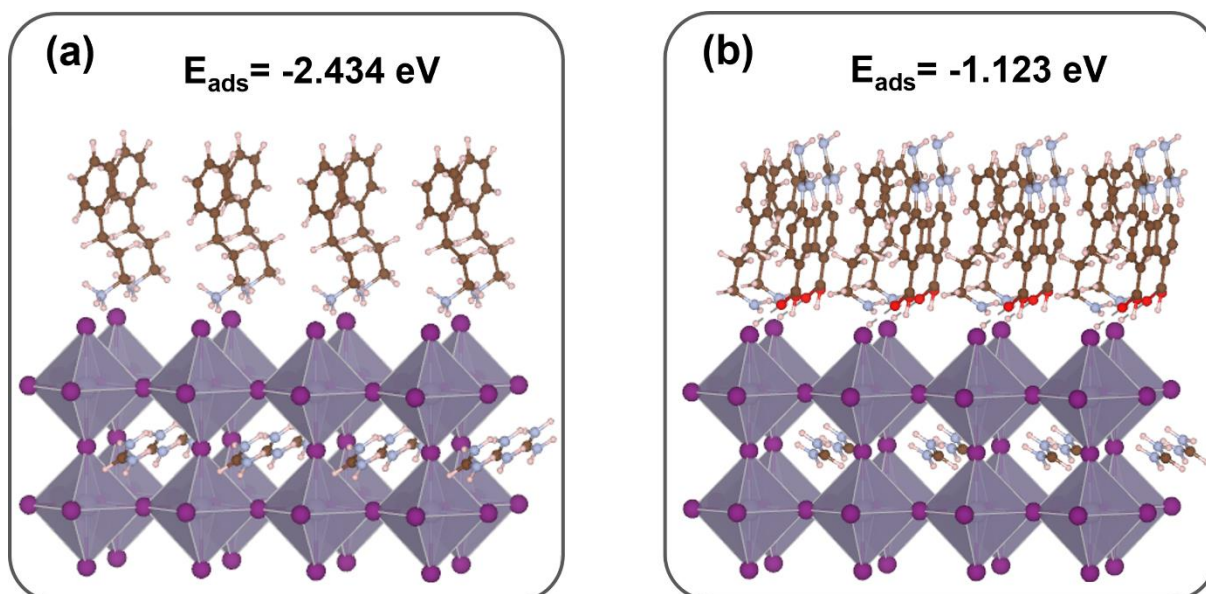
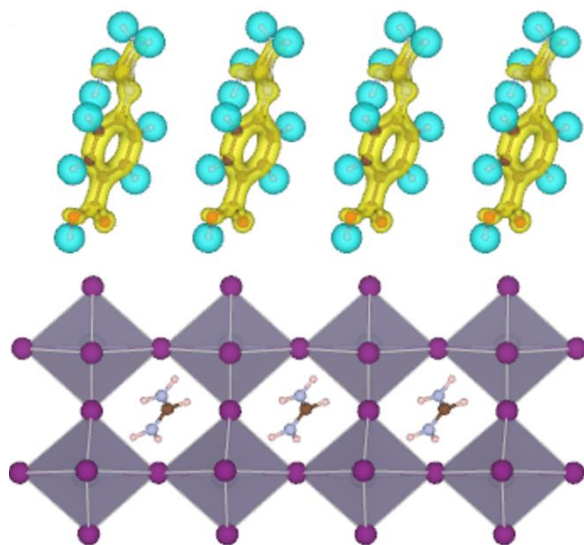


Fig. S2 The adsorption energy between the FASnI<sub>3</sub> and (a) PEA or (b) PEA-GBAC.



**Fig. S3** The electron density distribution of FASnI<sub>3</sub> interacting with GBAC.

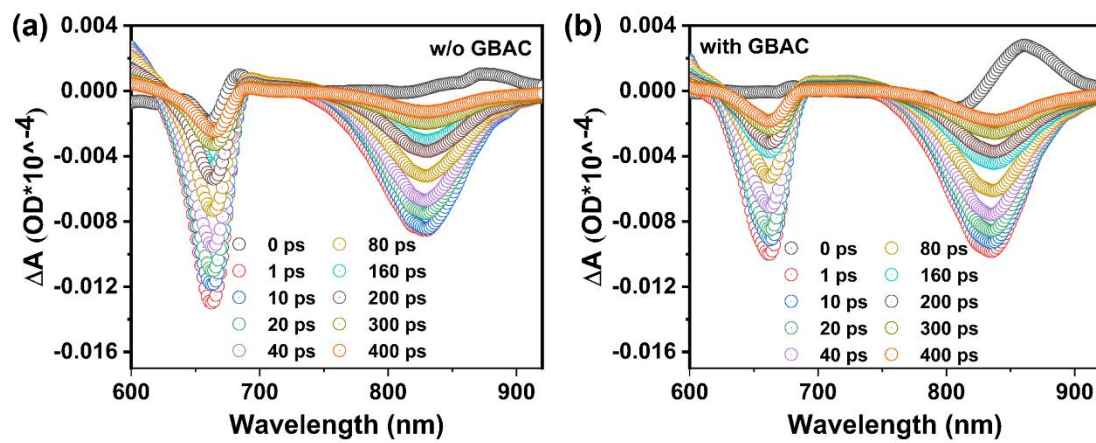


Fig. S4 The delay time-dependent TA spectra for perovskite films: (a) without GBAC, and (b) with GBAC.

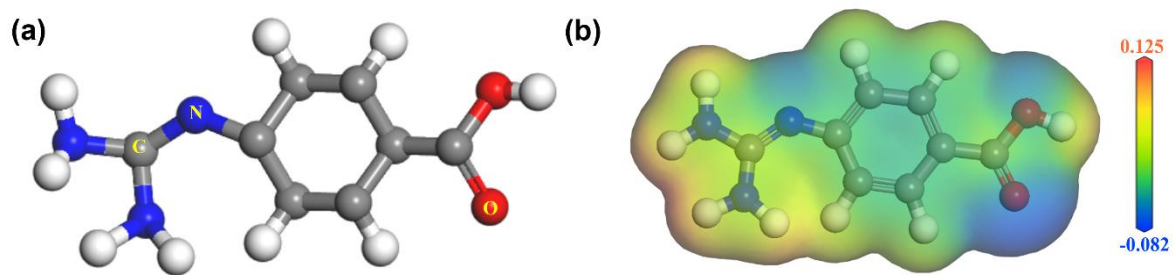


Fig. S5 Molecular structure and Electrostatic potential diagrams of GBAC.

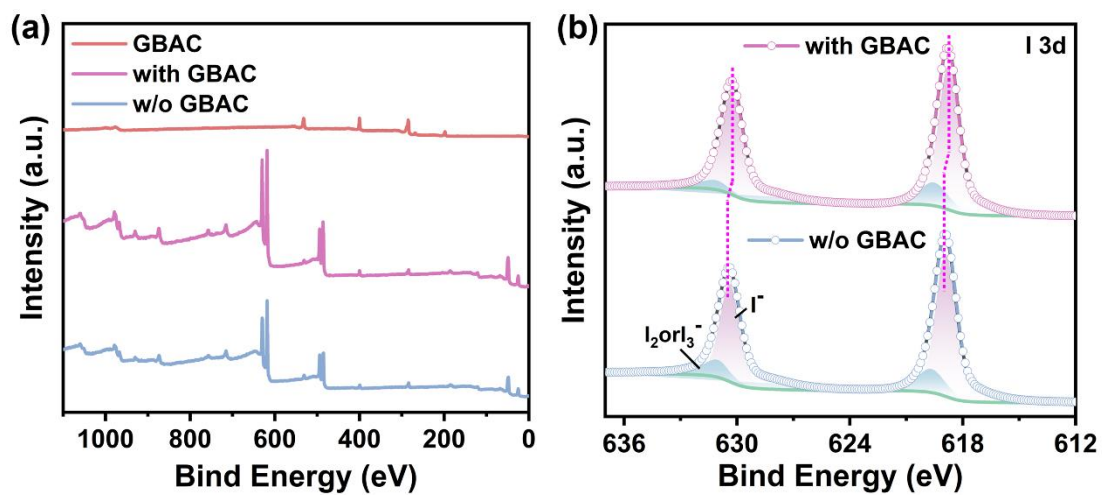


Fig. S6 (a) Full XPS spectra, and (b) High-resolution XPS spectra of I element of perovskite films without and with GBAC.

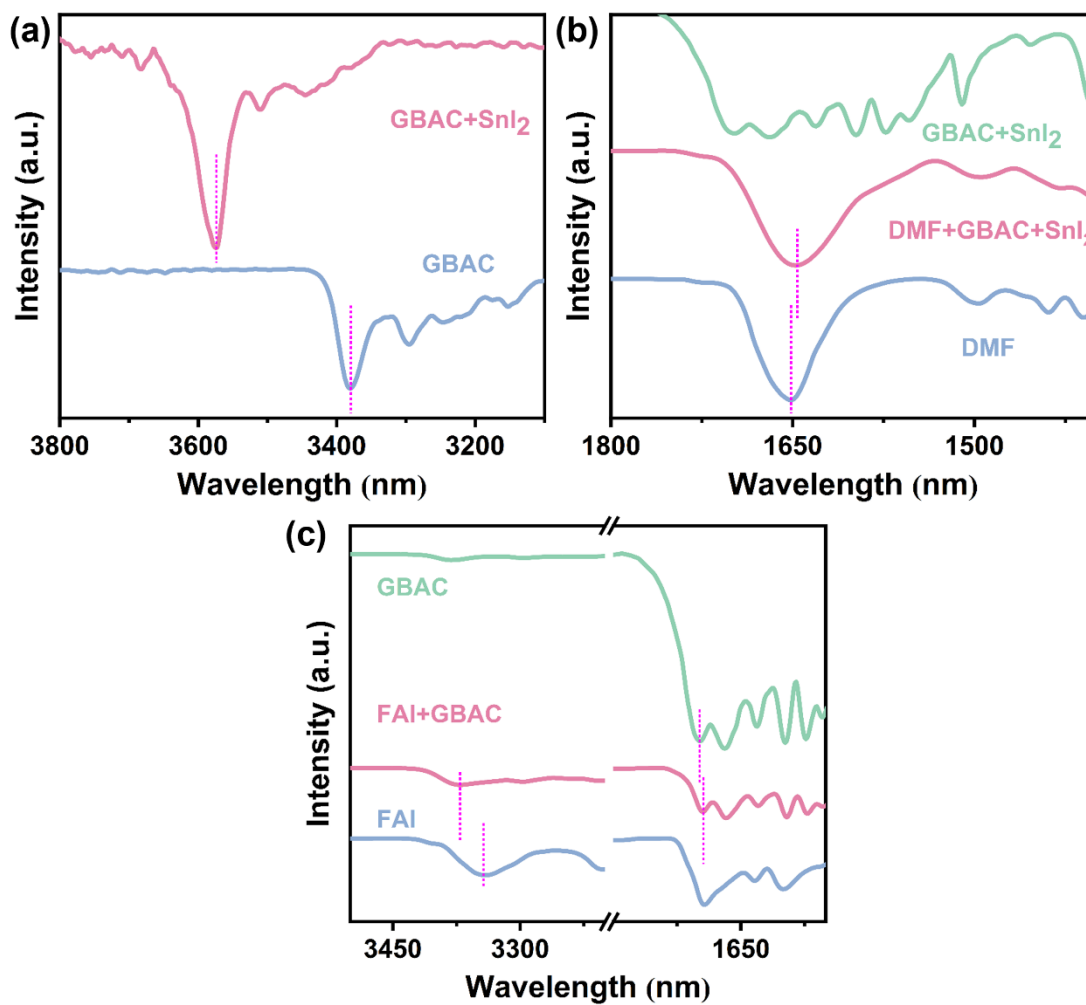


Fig. S7 FTIR spectra: (a) GBAC and GBAC+SnI<sub>2</sub>, (b) GBAC+SnI<sub>2</sub>, DMF+GBAC+SnI<sub>2</sub> and DMF, (c) GBAC, GBAC+FAI and FAI.

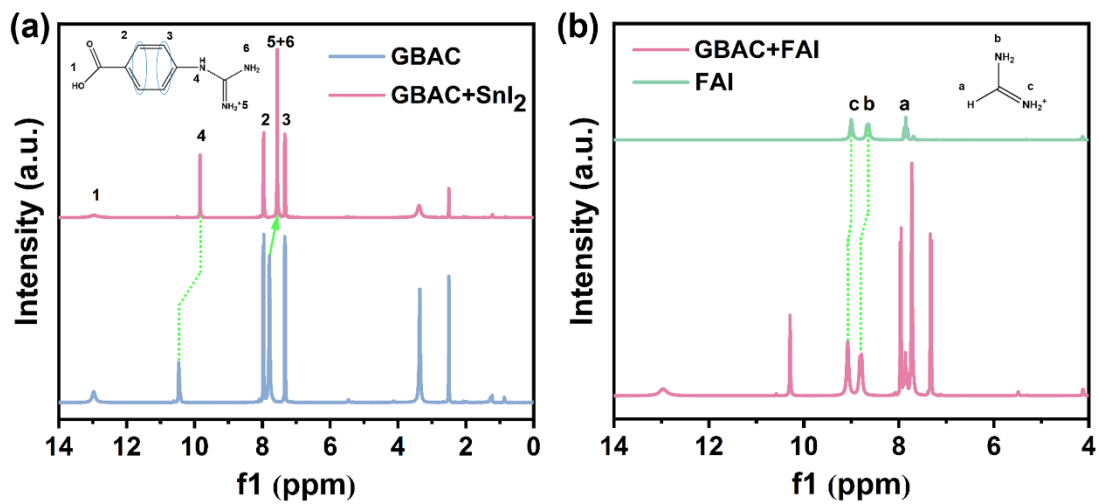
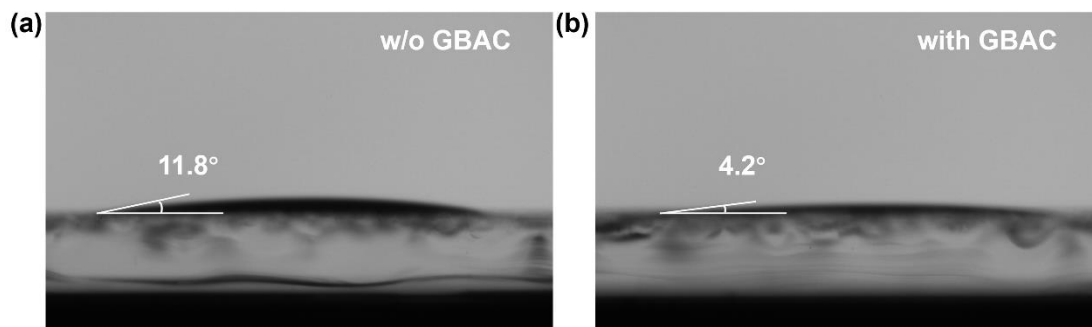
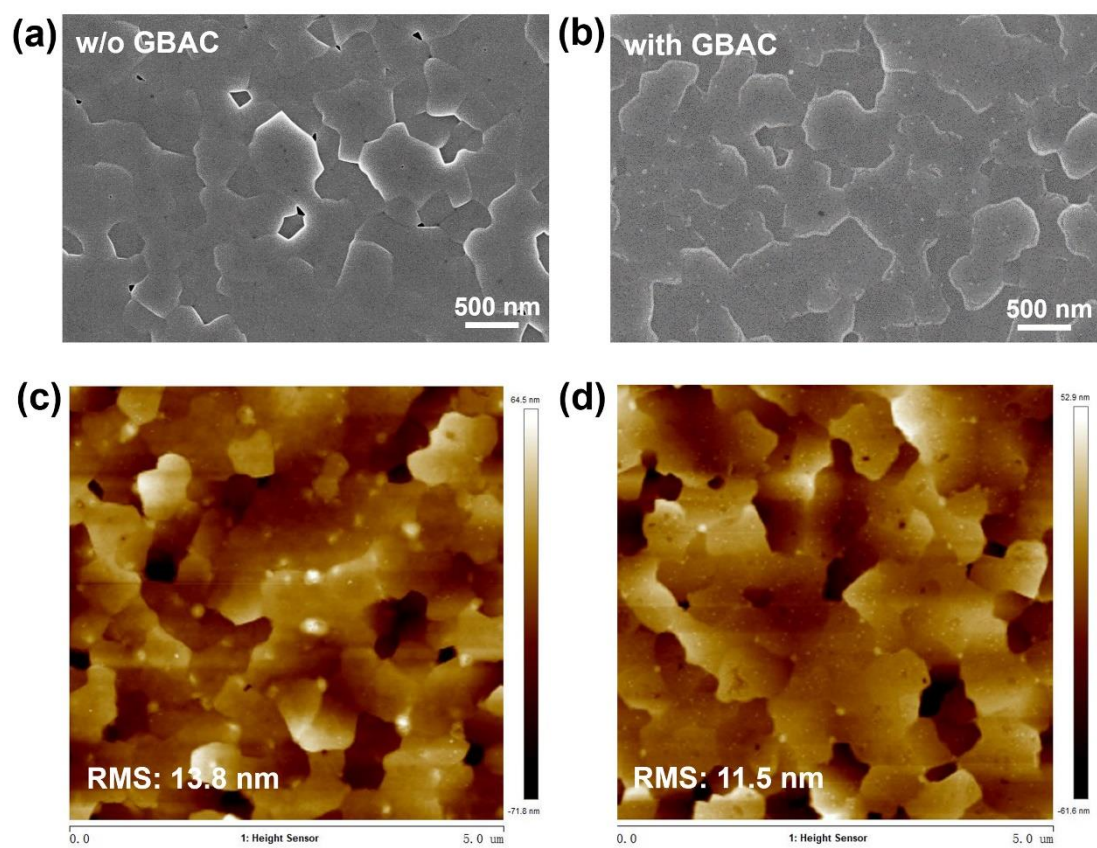


Fig. S8  $^1\text{H}$ NMR spectra: (a) GBAC and GBAC+ $\text{SnI}_2$ , (b) GBAC+FAI and FAI.



**Fig. S9** The contact angle of perovskite precursor on PEDOT: PSS: (a) without GBAC, (b) with GBAC.



**Fig. S10** SEM images of perovskite films: (a) without GBAC, (b) with GBAC. AFM images of perovskite films: (c) without GBAC, (d) with GBAC.

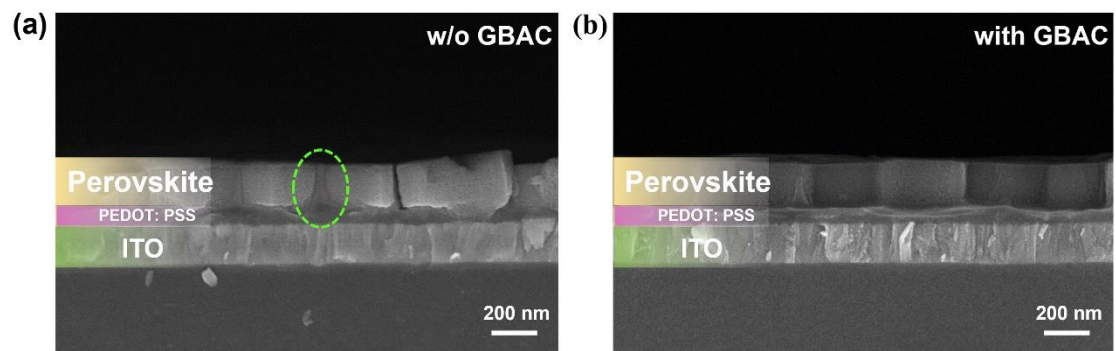


**Fig. S11** Cross-sectional SEM images of perovskite films: (a) without GBAC, (b) with GBAC.

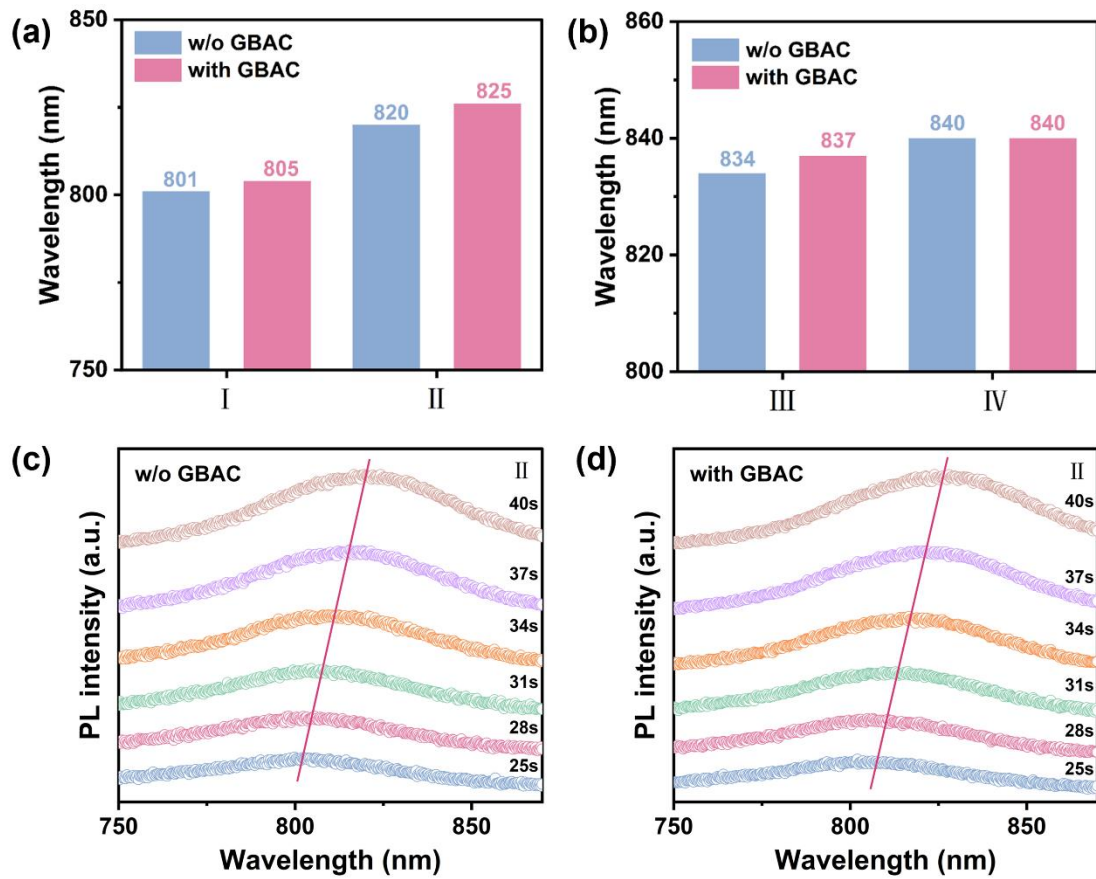


**Fig. S12** PL peak position at different stages for perovskite films without and with GBAC: (a) spin coating, (b) annealing. Time-dependent peak shift in the in-situ PL during stage II for perovskite films: (a) without GBAC, (b) with GBAC.

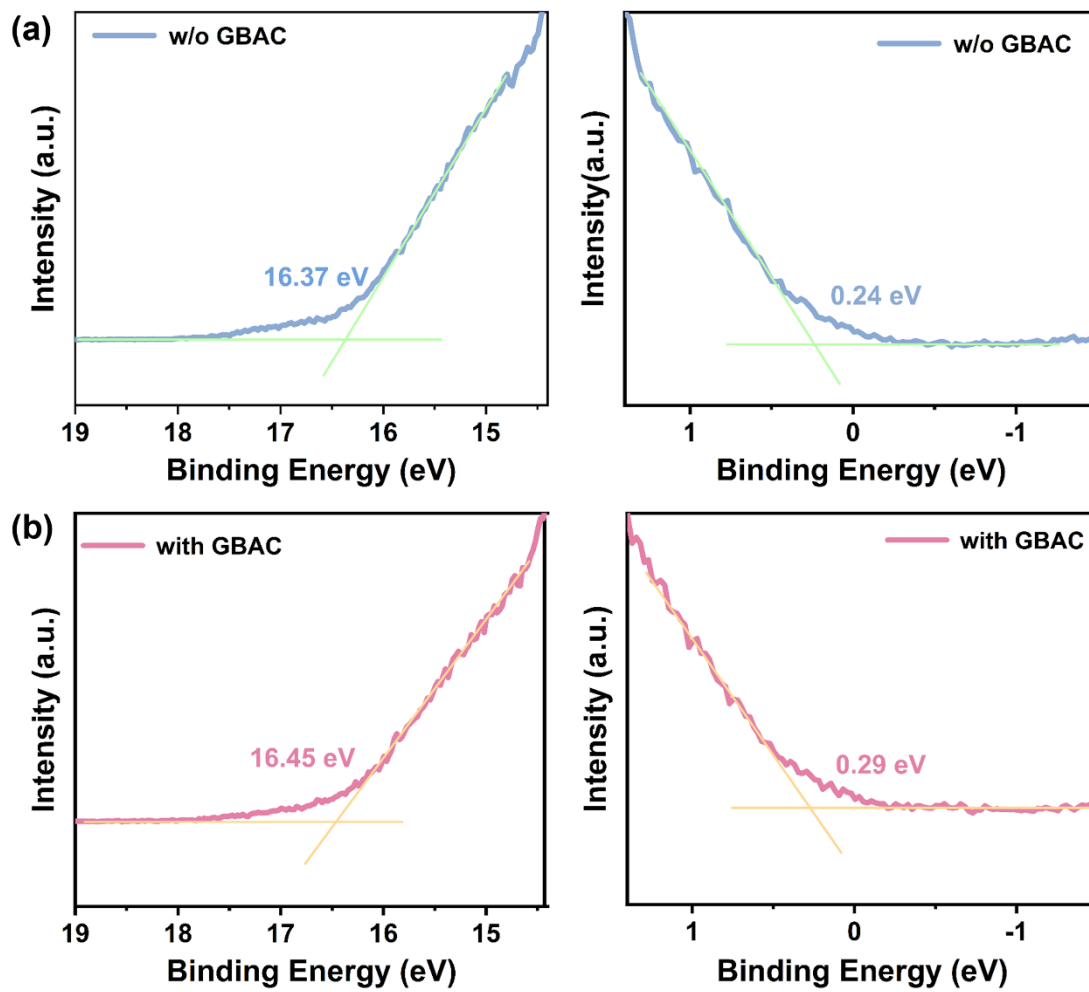
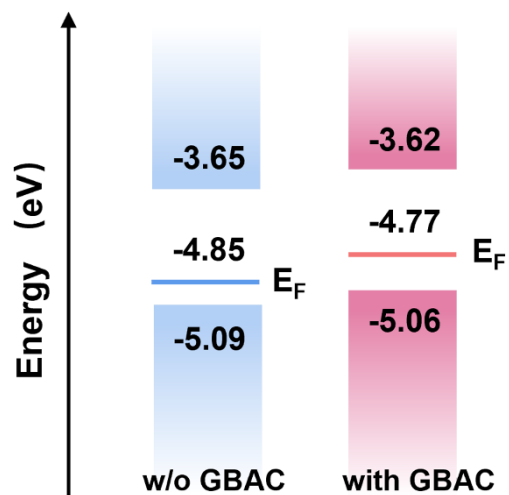
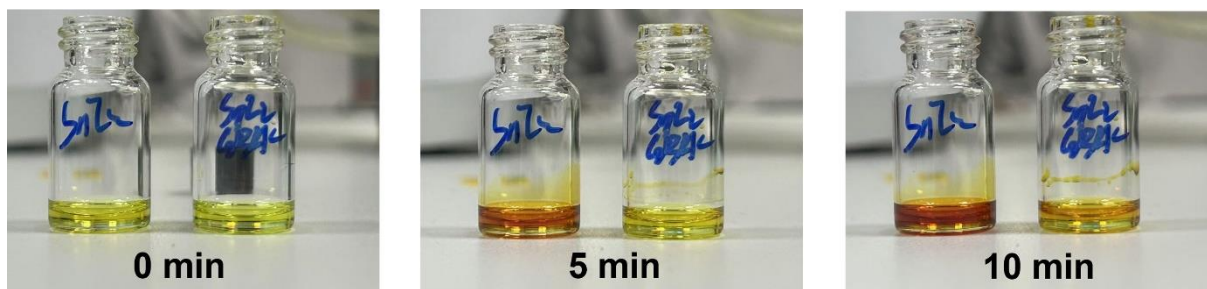


Fig. S13 UPS spectra of perovskite films measured with a photon energy of 21.2 eV: (a) without GBAC, (b) with GBAC.



**Fig. S14** The energy-level scheme of both perovskite films without and with GBAC based on the parameters derived from UPS spectra.



**Fig. S15** Oxidation state of SnI<sub>2</sub> and SnI<sub>2</sub>+GBAC upon exposed to air.

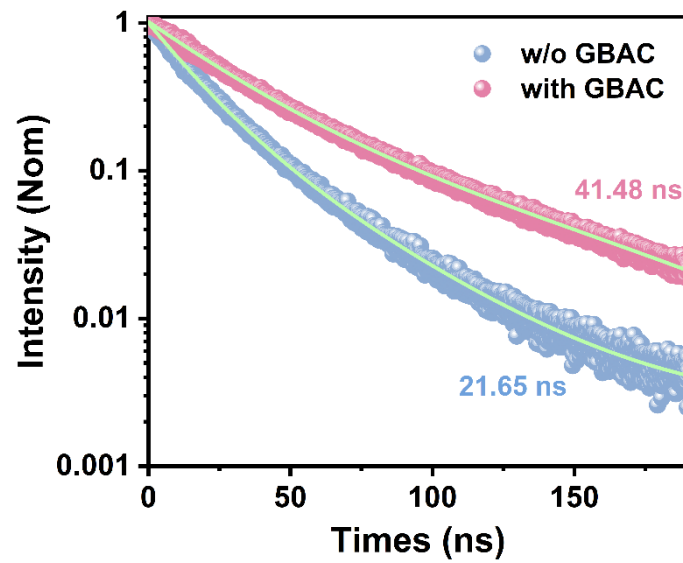
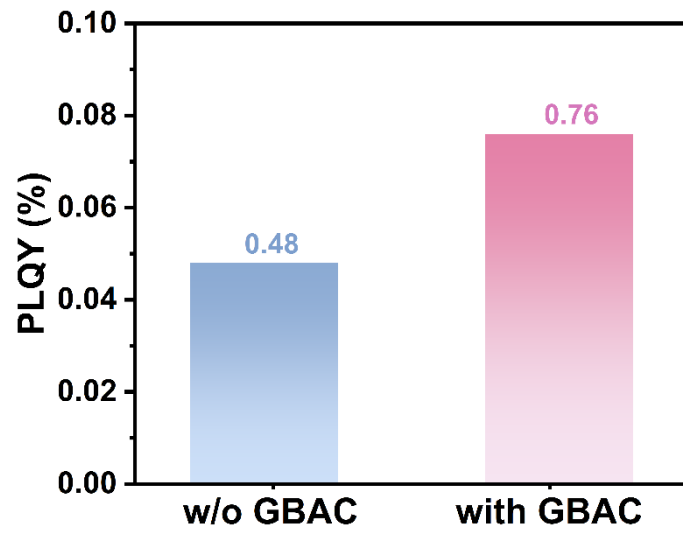


Fig. S16 TRPL spectra of perovskite films without and with GBAC.



**Fig. S17** The PLQY diagram of perovskite films without and with GBAC.

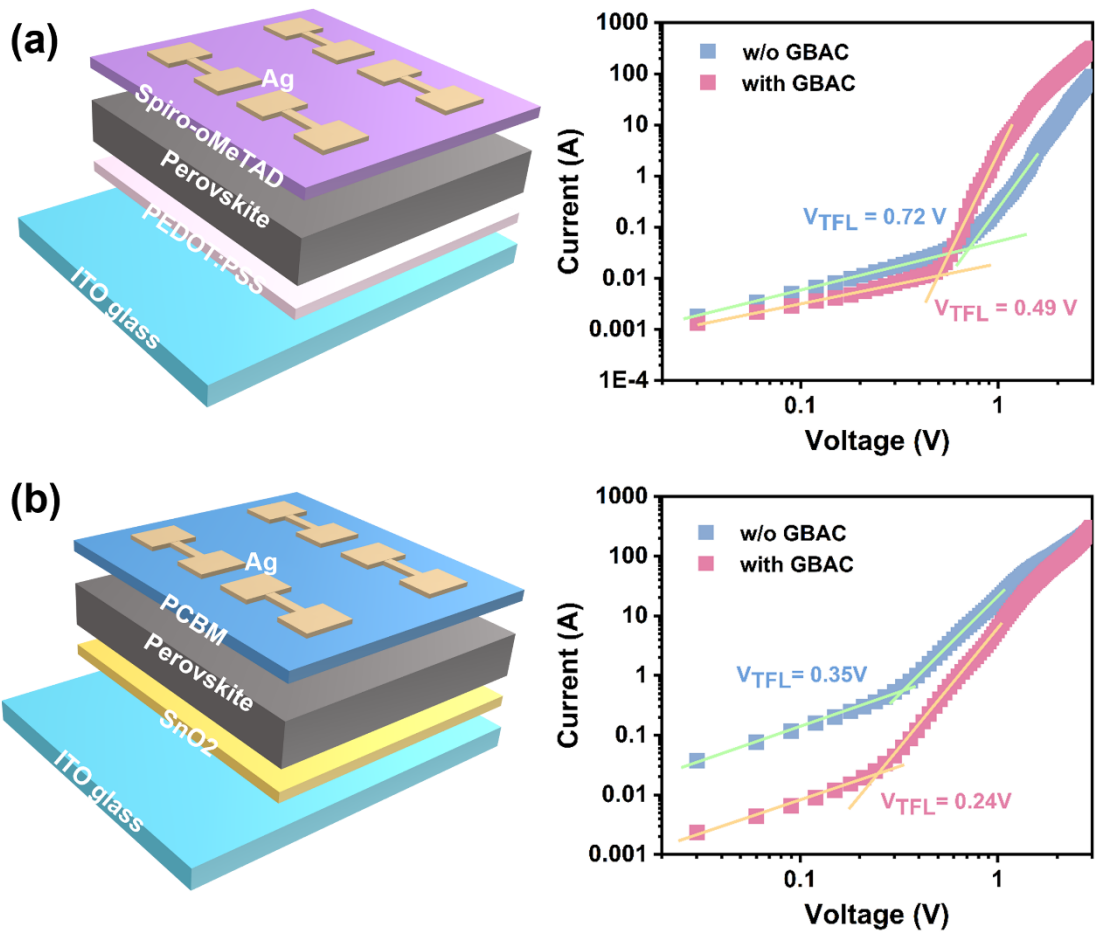
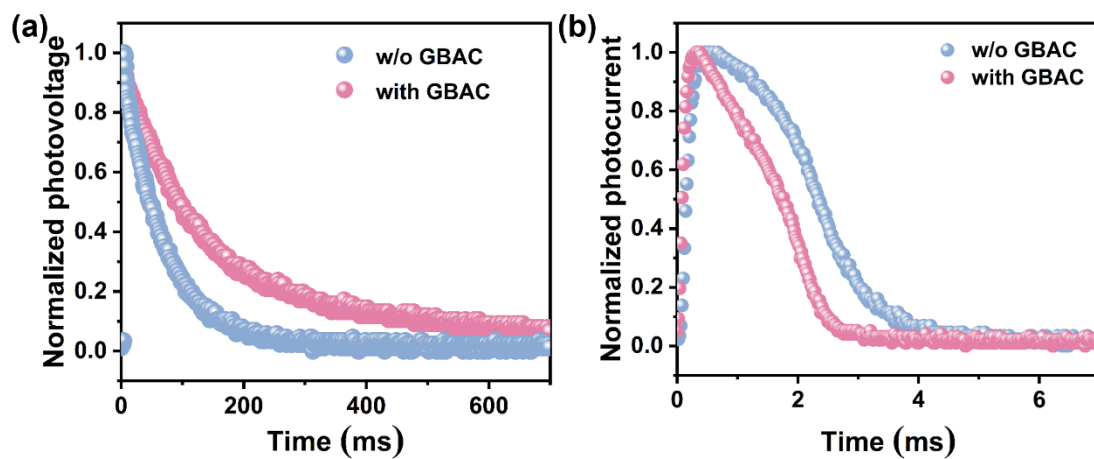


Fig. S18 Dark J-V curves of the devices: (a) electron-only, (b) hole-only.



**Fig. S19** (a) Transient photovoltage (TPV) and (b) transient photocurrent (TPC) decay measurements of PSCs based on perovskite films without and with GBAC.

**Table S1** High-resolution peak position of N, I, Sn, and O elements for perovskite films without and with GBAC.

<b>Sample</b>	<b>w/o GBAC (eV)</b>	<b>with GBAC (eV)</b>	<b>GBAC</b>
<b>N 1s</b>	400.28	400.40	400.25
<b>I 3d</b>	630.45	630.22	
	619.01	618.70	
<b>Sn</b>	495.09	494.80	
	486.65	486.40	
<b>O</b>	530.42	530.54	531.73

**Table S2** TRPL fitting parameters for perovskite films without and with GBAC.

<b>Sample</b>	$A_1$	$\tau_1$ (ns)	$A_2$	$\tau_2$ (ns)	$\tau_{ave}$ (ns)
<b>w/o GBAC</b>	0.80	28.54	0.20	93.25	41.48
<b>with GBAC</b>	0.70	15.32	0.30	36.43	21.65

**Table S3** The trap density derived from SCLC.

<b>Sample</b>	<b>Single electron devices (cm<sup>-3</sup>)</b>	<b>Single hole devices (cm<sup>-3</sup>)</b>
<b>w/o GBAC</b>	1.99 $\times$ 10 <sup>15</sup>	4.10 $\times$ 10 <sup>15</sup>
<b>with GBAC</b>	1.37 $\times$ 10 <sup>15</sup>	2.79 $\times$ 10 <sup>15</sup>

**Table S4** Statistical photovoltaic parameters for both tin PSCs.

<b>Sample</b>	<b>V<sub>oc</sub> (V)</b>	<b>FF (%)</b>	<b>J<sub>sc</sub> (mA/cm<sup>2</sup>)</b>	<b>PCE (%)</b>
<b>w/o GBAC</b>	0.77±0.03	68.98±1.72	21.56±0.64	11.21±0.57
<b>with GBAC</b>	0.87±0.03	72.76±0.96	22.98±0.48	14.52±0.50

**Table S5** A summary of the photovoltaic parameters of high-efficiency tin PSCs reported in recent two years (2023-2024).

Device Structure	$V_{oc}$ (V)	$J_{sc}$ (mA/cm <sup>2</sup> )	FF (%)	PCE (%)	Ref
ITO/PEDOT:PSS/ PEA <sub>0.15</sub> FA <sub>0.85</sub> SnI <sub>3</sub> /ICBA/BCP/Ag	1.01	18.89	73.21	14.02	2023 <sup>6</sup>
FTO/PEDOT:PSS/Sn/ (Cs <sub>0.02</sub> (FA <sub>0.9</sub> DEA <sub>0.1</sub> ) <sub>0.98</sub> ) <sub>0.98</sub> EDA <sub>0.01</sub> I <sub>3</sub> /SnOx/C60/Ag.	0.77	25.18	0.74	14.31	2023 <sup>7</sup>
ITO/PEDOT:PSS/ pF-PEAFA <sub>0.8</sub> SnI <sub>3</sub> /ICBA/BCP/Ag	0.95	22.15	69.10	14.53	2023 <sup>8</sup>
ITO/PEDOT:PSS/ (Cs <sub>0.025</sub> (MA <sub>0.25</sub> FA <sub>0.75</sub> ) <sub>0.975</sub> ) 0.98EDA <sub>0.01</sub> SnI <sub>3</sub> /C60/BCP/Ag	0.83	23.84	73.74	14.41	2023 <sup>9</sup>
ITO/PEDOT:PSS/ DFPD <sub>2</sub> SnI <sub>4</sub> /FASnI <sub>3</sub> /C60/BCP/Ag	0.81	23.24	71.23	13.34	2023 <sup>10</sup>
ITO/PEDOT:PSS/ PEA <sub>0.2</sub> FA <sub>0.8</sub> SnI <sub>3</sub> /ICBA/BCP/Ag	0.97	20.02	73.00	14.20	2024 <sup>11</sup>
ITO/PEDOT:PSS/ PEA <sub>0.15</sub> FA <sub>0.85</sub> SnI <sub>3</sub> /ICBA/BCP/Ag	0.80	22.28	77.80	13.90	2024 <sup>12</sup>
ITO/PEDOT:PSS/PEA <sub>0.15</sub> FA <sub>0.85</sub> SnI <sub>3</sub> /PCBM/BCP/Ag	0.86	24.81	72.37	15.38	2024 <sup>13</sup>
ITO/PEDOT:PSS/ (3-TEA) <sub>0.2</sub> FA <sub>0.8</sub> SnI <sub>3</sub> /ICBA/BCP/Ag	0.89	23.71	67.02	14.16	2024 <sup>14</sup>
ITO/NiO <sub>x</sub> / PEA <sub>0.2</sub> FA <sub>0.8</sub> SnI <sub>3</sub> /ICBA/BCP/Ag	0.94	20.92	73.23	14.27	2024 <sup>15</sup>
ITO/PEDOT:PSS/ (3-TEA) <sub>0.2</sub> FA <sub>0.8</sub> SnI <sub>3</sub> /ICBA/BCP/Ag	0.97	21.70	74.10	15.70	2024 <sup>16</sup>
ITO/PEDOT:PSS/ TEA <sub>0.2</sub> FA <sub>0.8</sub> SnI <sub>3</sub> /ICBA/BCP/Ag	0.97	20.12	76.61	15.04	2024 <sup>17</sup>
ITO/PEDOT:PSS/ PEA <sub>0.2</sub> FA <sub>0.8</sub> SnI <sub>3</sub> /ICBA/BCP/Ag	0.97	21.58	72.29	15.13	2024 <sup>18</sup>
ITO/PEDOT:PSS/ FASnI <sub>3</sub> /ICBA/BCP/Ag	0.80	23.13	76.71	14.13	2024 <sup>19</sup>
ITO/PEDOT:PSS/ FA <sub>0.75</sub> MA <sub>0.25</sub> SnI <sub>2.75</sub> Br <sub>0.25</sub> /C60- ETPA/BCP/Ag	0.91	21.16	69.22	13.28	2024 <sup>20</sup>
ITO/PEDOT:PSS/pF-PEAFA <sub>0.8</sub> SnI <sub>3</sub> /ICBA/BCP/Ag	0.96	21.67	70.94	14.78	2024 <sup>21</sup>
ITO/PEDOT:PSS/PEA <sub>0.15</sub> FA <sub>0.85</sub> SnI <sub>3</sub> (GBAC)/PCBM/BCP/A g	0.88	23.20	73.72	15.02	This Work

## References

1. P. E. Blöchl, *Phys. Rev. B*, 1994, **50**, 17953.
2. X. Meng, Q. Sun, B. Shen, D. Hu, B. Kang, S. R. P. Silva and L. Wang, *Small*, 2024, **20**, 2310275.
3. S. C. Feng, Y. Shen, X. M. Hu, Z. H. Su, K. Zhang, B. F. Wang, L. X. Cao, F. M. Xie, H. Z. Li, X. Gao, J. X. Tang and Y. Q. Li, *Adv Mater*, 2024, **36**, 2410255.
4. Z. Kang, S. Wang, T. Seto and Y. Wang, *Adv. Opt. Mater*, 2021, **9**, 2101173.
5. Q. Dong, Y. Fang, Y. Shao, P. Mulligan, J. Qiu, L. Cao and J. J. S. Huang, *Science*, 2015, **347**, 967-970.
6. G. Liu, X. Jiang, W. Feng, G. Yang, X. Chen, Z. Ning and W. Q. Wu, *Angew. Chem. Int. Ed*, 2023, **62**, e202305551.
7. L. Wang, Q. Miao, D. Wang, M. Chen, H. Bi, J. Liu, A. K. Baranwal, G. Kapil, Y. Sanehira, T. Kitamura, T. Ma, Z. Zhang, Q. Shen and S. Hayase, *Angew. Chem. Int. Ed*, 2023, **62**, e202307228.
8. F. Hu, C. H. Chen, T. Y. Teng, Y. R. Shi, B. Wang, D. Xue, Y. Xia, J. Chen, K. L. Wang, L. Z. Huang, I. Yavuz, Z. K. Wang and L. S. Liao, *Adv. Energy Mater*, 2024, **14**, 2302926.
9. Y. Zhang, B. Zhao, L. Liu, J. Zhou, X. Ma and N. Wang, *Small*, 2023, **20**, 2306115.
10. B. Chang, L. Wang, H. Li, L. Pan, Y. Wu, Z. Liu, Y.-N. Zhang, E. Guo and L. Yin, *ACS Energy Lett*, 2024, **9**, 363-372.
11. G. Liu, X. Jiang, Y. He, C. H. Kuan, G. Yang, W. Feng, X. Chen and W. Q. Wu, *Angew. Chem. Int. Ed*, 2024, **64**, 202419183.
12. F. He, T. Li, T. Shen, Y. Zhao, Z. Jin, Z. Zhang, Y. Pu, L. Deng, L. Qin, Y. Zhan, Y. Liu, Y. Wang and J. Liang, *Adv. Funct. Mater*, 2024, **34**, 2405611.
13. J. Chen, J. Luo, E. Hou, P. Song, Y. Li, C. Sun, W. Feng, S. Cheng, H. Zhang, L. Xie, C. Tian and Z. Wei, *Nat. Photon*, 2024, **18**, 464-470.
14. G. Feng, H. L. Loi, T. Wang, W. Deng, Z. Guan, Q. Wei, J. He, M. Li, C. S. Lee, J. Wang, Q. Zhang and F. Yan, *Angew. Chem. Int. Ed*, 2025, **64**, e202413584.
15. T. Wang, H. L. Loi, Q. Cao, G. Feng, Z. Guan, Q. Wei, C. Chen, M. Li, Y. Zhu, C. S. Lee and F. Yan, *Adv Mater*, 2024, **36**, 2402947.
16. Y. Shi, Z. Zhu, D. Miao, Y. Ding and Q. Mi, *ACS Energy Lett*, 2024, **9**, 1895-1897.
17. M. Ma, X. Jiang, Z. Zang, X. Wen, W. Zhou, H. Wu, S. Peng, Y. Liu, H. Li, D. Yu, H. Liang, H. Wang, W. Zhou, Z. Su, F. Zheng, X. Gao, A. V. Emeline, C. C. Stoumpos and Z. Ning, *Adv. Funct. Mater*, 2024, **34**, 2407095.
18. J. Wang, J. Huang, M. Abdel-Shakour, T. Liu, X. Wang, Y. Pan, L. Wang, E. Cui, J. S. Hu, S. Yang and X. Meng, *Angew. Chem. Int. Ed*, 2024, **63**, e202317794.
19. J. Jin, Z. Zhang, S. Zou, F. Cao, Y. Huang, Y. Jiang, Z. Gao, Y. Xu, J. Qu, X. Wang, C. Chen, C. Xiao, S. Ren and D. Zhao, *Adv. Energy Mater*, 2024, 2403718.
20. S. Wang, C. Wu, T. Wu, H. Yao, Y. Hua and F. J. A. E. L. Hao, *ACS Energy Lett*, 2024, **9**, 1168-1175.
21. Y. T. Yang, F. Hu, T. Y. Teng, C. H. Chen, J. Chen, N. Nizamani, K. L. Wang, Y. Xia, L. Huang and Z. K. Wang, *Angew. Chem. Int. Ed*, 2024, **137**, e202415681.